Journal of Nondestructive Evaluation, Vol. 20, No. 1, 2001

The Potential of Guided Waves for Monitoring Large Areas of Metallic Aircraft Fuselage Structure

R. P. Dalton, P. Cawley, and M. J. S. Lowe

Received October 9, 2000

The potential for long-range propagation of ultrasonic guided waves through metallic aircraft fuselage structure has been investigated using dispersion analysis and numerical modelling, validated by experiment. In order to satisfy the pressing need for integrated structural health monitoring of ageing metallic aircraft, it is likely that an active guided wave system based on current technology must feature efficient propagation over distances of at least 1m with an attenuation of not more than about 40dB/m. Propagation was examined across free skin, tapering skin, skin loaded with sealant and paint, double skin jointed with either sealant or adhesive, and lap and stringer joints, which together adequately characterise metallic monocoque fuselage construction. Whilst the simple and tapering skins allow long range propagation of non-dispersive modes with little reflection at the transition to tapering skin, the attenuation caused by application of a sealant layer generally leaves no viable modes. Guided wave propagation through double skin features the inevitable generation of twin modes with similar phase velocity, which interact with each other during propagation. This interaction crucially determines the efficiency of propagation across narrow joints and effectively precludes propagation across a succession of joints. This work leads to the conclusion that an active aircraft system that relies on guided wave propagation of more than 1m is not feasible, whereas localised guided wave monitoring of structurally significant areas is a more practical approach.

KEY WORDS: Ultrasonics; guided waves; aircraft fuselage.

1. INTRODUCTION

A fully automated onboard system to monitor the structural health of an aircraft has the potential to reduce operating costs, increase flight safety, improve aircraft availability and, in the case of military aircraft, improve survivability. It is not surprising, therefore, that considerable effort is currently being focused on the development of such a system. The Aloha Airlines incident of April 1988[1] cast doubt upon the airworthiness of ageing metallic aircraft fleets and focused attention on the urgent need for an integrated structural health monitoring system that could be retro-fitted to these aircraft. Since the incident, a great deal of research effort has been directed to improving and developing non-destructive evaluation techniques to address this problem; however, only a small proportion of this work was concerned with development of an integrated system. Of the relatively few methods that are contenders for implementation into an integrated health-monitoring system, acoustic emission (AE) is probably the most developed. Commercial AE systems that are not permanently fitted, but are nevertheless designed to monitor the entire fuselage of a small airliner, have been available since the late nineteen eighties.[2] Recently AE has been placed on a more scientific footing with the consideration of event signals in terms of propagating guided modes, in what is now generally called 'modal acoustic emission'.[3] Spillman[4] and others believe that

Dept of Mechanical Engineering, Imperial College of Science Technology and Medicine, Exhibition Road, London, SW7 2BX, England.

0195-9298/01/0300-0029$19.50/0

optical methods offer the best means of implementing global health monitoring of aircraft, since optical sensors offer wide bandwidth, are structurally less intrusive, and can be configured to provide long gauge length sensing. Such a system would sense damage indirectly through an incidental parameter such as strain. A hybrid system utilising guided ultrasonic waves received by optical transducers has also been suggested.[5]

Owing to their unique potential for long-range, in-plane propagation through thin plates, guided waves seem to offer an obvious solution. The overriding issue concerning the implementation of such a system is the selection of suitable modes from the potentially infinite number that can exist. Regardless of the design of the transducer system, the efficiency of the system will depend heavily on minimising the transducer density, so efficient propagation through the structure is of prime importance. This paper examines the potential of guided waves for this application, by focusing on their propagation through metallic fuselage structure.

2. ESSENTIAL SYSTEM SPECIFICATIONS

The variation in aircraft performance and usage together with the complexity of aircraft structural design makes the task of defining general specifications for a structural health-monitoring system (SHMS) very difficult. However, under the American Joint Air Force contract: 'Smart Structures Concept Requirements' (SSCORE) an attempt was made by the Northrop corporation to outline some basic system requirements for military aircraft.[6] A global system was envisaged with rugged, reliable, sensors, capable of detecting cracks of 0.05 inches in length (~1.25 mm) in geometrically complex locations, close to fastener holes, apertures and sharp edges. This is a very demanding specification indeed. Since even spectral methods have difficulty resolving objects spaced at less than about half a wavelength, this implies a maximum wavelength of 2.5 mm to meet the SSCORE specification, which seemed rather ambitious. In this investigation, for the purposes of rejecting impractical modes, a somewhat arbitrary maximum wavelength limit of 15 mm was set for the selection of potentially useful modes.

A rough estimate of the fuselage surface area of the relatively small Boeing 737 aircraft indicated that for a transducer pitch of one meter, about 400 transducers would be required and for a Boeing 747, four times this number would be needed. It was consequently decided that efficient propagation over at least a meter was an essential requirement. From the findings of recent development work for guided-wave pipe inspection systems,[7] defect echoes of roughly −20 dB are required and, based on current transducer technology, an initial signal-to-noise ratio of about 60 dB may be assumed. It was therefore decided that the signal should decay by no more than 40 dB over the propagation distance. The primary objective therefore was to identify modes with wavelengths of no more than 15 mm having an effective attenuation of less than 40 dB/m. The strategy employed was to use these somewhat arbitrary and subjective limits to net all potentially viable modes, given that long range propagation underpins the viability of any mode. A further selection might then be made based on other factors such as defect sensitivity, excitability and interaction with fasteners.

3. CHARACTERISATION OF AIRCRAFT STRUCTURE

It is fortunate that the group of metallic ageing aircraft in which we are interested generally exhibits little variation in construction, in terms of the arrangement of components and the materials used. Although some steel, titanium and magnesium alloys are found, the vast majority of the structure is composed of aluminium alloy in forged and plate form. The alloy chosen to represent aircraft skin was 2014, which is commonly used for fuselage skins. Semi-monocoque fuselage skins are by definition supported by a sub-structure of frames and stringers as shown in Fig. 1. Often the same material is used for both the sub-structural components and the skin, and for simplicity this assumption was adopted. It was also assumed, for simplicity, that the material thicknesses of the skin and sub-structure are the same. The thickness of a single layer of fuselage skin varies, but a skin thickness

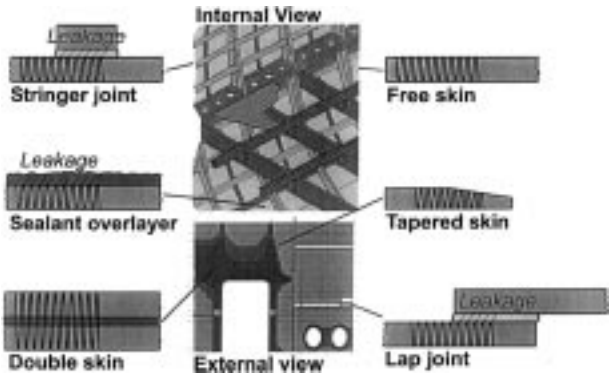

Fig. 1. Semi-monocoque fuselage construction and the structural features examined.

of 16 swg (1.63mm) or 18 swg (1.22 mm) is commonly found in commercial aircraft and the latter was adopted for the generic skin in this project.

The general method of fuselage construction is described by Megson.[8] Anti-corrosion treatment and primer paint is applied to structural components before assembly and a jointing compound is usually applied between riveted joints. One of the most common jointing compounds used is PRC, a polysulphide sealant that is also used to seal integral fuel tanks. In fuel tanks the sealant is applied to the internal surface along the joint lines, and sealant is often daubed over the rivet heads to a depth of up to 5mm. The thickness of the jointing layer in riveted joints was found to be thinner close to the rivets, but away from the rivets the joint thickness was fairly consistent at 0.3 mm. It was felt that, to simplify initial analysis, rivets should be excluded, so for the purposes of this investigation a standard sealed joint would feature a jointing layer of PRC 1442-B2 with a thickness of 0.3mm. In some aircraft the stringers are bonded to the skin rather than riveted. Lap joints between skins, and the sub-structure-to-skin joints, may be both bonded and riveted. A number of different adhesives have been used, the most popular being AF163 and Redux 775. Redux adhesive, supplied in film form and cured under conditions set out in the DTD 775B specification, was used throughout this investigation. It was found that when cured, the jointing layer had a mean thickness of 0.25 mm which defined the nominal thickness of a bonded joint.

Much of the work involved predictions of mode attenuation, using the program: 'Disperse' developed at Imperial College[9] and verification by selected experimental measurements. The acoustic properties of the materials chosen to represent those used in generic aircraft construction were obtained from literature or measured, in order to facilitate the predictions, and the results are shown in Table I.

The complexity of the fuselage structure illustrated in Fig. 1 is formidable and in order to simplify the problem a number of essential structural features were identified, which together characterise the semi-monocoque fuselage of any aircraft. Although the density of structural features is high, almost all fall into one of the six types shown in Fig. 1, each of which presents a different guided wave system. These features are somewhat idealised, since their essential function is simply to provide insight into the signal propagation. Such idealisation was necessary in order to reduce the structural permutations to a manageable set, without unduly compromising the relevance of the results.

Propagation across each of the structural features will be discussed in turn and it should be remembered that long range propagation was the primary concern and that only cursory reference is made to possible defect resolution and mode isolation, either of which may preclude practical use of any given mode.

4. PROPAGATION IN A FREE SKIN

The propagation of Lamb waves in the isotropic free plate is a mature subject with an exhaustive literature base. Defect sensing for this system has also been very thoroughly researched both theoretically and experimentally. (See, for example, [10–12]). Mode selection begins with consideration of the dispersion curves, which are shown in Fig. 2.

4.1 Mode Selection Factors

Minimising attenuation is of paramount importance in the selection of modes for long-range applications. In the aluminium free plate there are four mechanisms of Lamb wave attenuation, only two of which are significant, and determine the propagation efficiency.[13] Dispersion is the tendency of a signal to spread spatially and temporally during propagation, owing to the differing velocities of its frequency components. This broadening distribution of energy gives rise to a drop in signal amplitude. Non-

Table I. Acoustic properties of aircraft skin system materials

Structure	Material	Spec.	Density (kg/m^3)	Longitudinal velocity (m/s)	Shear velocity (m/s)	Longitudinal Attenuation (np/λ)	Shear Attenuation (np/λ)
Skin	Duralumin	BS L157	2700**	6348**	3133**	negligible*	negligible*
Jointing/Sealant	Polysulfide Sealant	PRC 1422B2	1527	1500	200	0.2	1***
Bonding Adhesive	Phenol-formaldehyde polyvinyl-formal	REDUX 775	1036	2829	1325	0.12	0.29

*compared with the other materials **Published data ***Assumed (too high to measure)

dispersive mode points, indicated in Fig. 2 (b), are defined by maxima and minima on the group velocity spectrum of which maxima are to be preferred. These issues are discussed fully by Alleyne and Cawley[14] and Wilcox *et al.*[13] Beam-spread is a function of both the transduction system and the frequency selected, and is fundamentally a diffraction phenomenon. The wavefronts of signals excited by finite sources extend with propagation distance, causing a spreading of energy and consequent loss of amplitude. The remaining attenuation mechanisms are the material attenuation, which includes scatter and viscoelastic factors, and attenuation owing to leakage of energy into the surrounding air. Both these mechanisms cause insignificant attenuation in the free plate, but are of critical importance in the multi-layered systems considered later.

The degree to which a mode can be isolated during excitation is another important factor discussed by Alleyne and Cawley[14] who stressed the importance of single mode operation. To excite a single mode, both the phase velocity (or wavenumber) and frequency bands of excitation must be constrained sufficiently to exclude unwanted modes. Mode conversion to other modes within the bandwidth of the incident signal is an inevitable consequence of guided wave interaction with structural features and since the number of possible modes increases with frequency, lower bands may be preferred. In later sections it will be shown that mode conversion favours modes with similar phase velocity to that of the incident mode and this is a further reason for selecting modes that are well isolated in the phase velocity spectrum. This issue plays an important part in the analysis of multi-layered systems and will be discussed more fully in later sections.

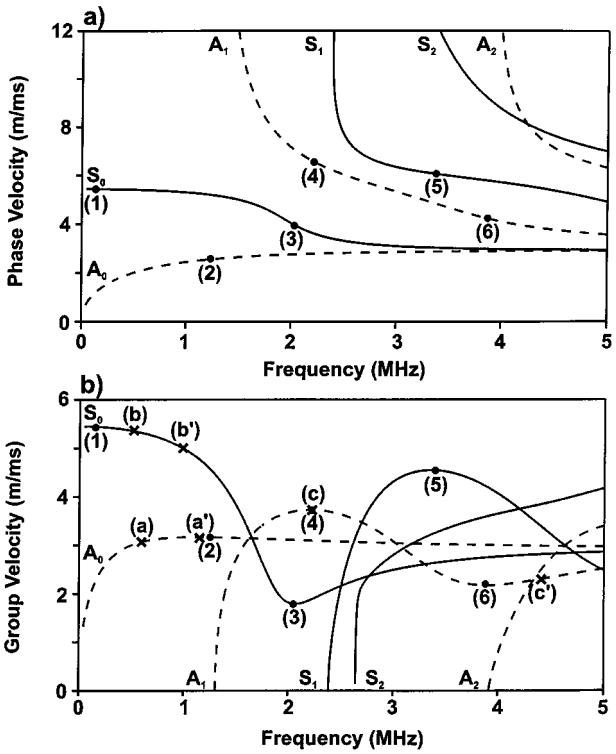

Fig. 2. a) Phase velocity and b) Group velocity spectra for Lamb modes in an aircraft skin (1.2 mm thick). Non-dispersive points are numbered and other points are referred to in the text. (- - - - - : Anti-symmetric modes, ——— : Symmetric modes.)

Finally consideration must be given to the distribution of particle displacement through the plate thickness, called the mode shape. This is important when assessing defect sensitivity, an issue that is not considered in this paper. However, the mode shape also has a bearing on the excitation of a given mode. Transduction methods that apply out-of-plane forces at the plate surface will only couple to modes exhibiting significant surface out-of-plane displacement.

In the case of a simple skin, provided that dispersion is controlled by selection of a non-dispersive point and the bandwidth of the signal is constrained to this non-dispersive region, then attenuation will be well within the 40dB/m limit. The low frequency non-dispersive regions on the A_0 and S_0 modes (0.9–1.8 MHz-mm and $<$0.5 MHz-mm respectively) are particularly useful owing to their relative isolation from other modes.

5. TAPERING SKIN

A short investigation of tapering skin was carried out simply to establish the level of reflection from the change in section that detracts from the transmitted signal energy and tends to complicate the received signal. Analytical study of tapering waveguides is difficult and appears to be limited to early and somewhat crude one-dimensional approximations for the acoustic field in a rectangular horn (see, for example, [15]). A numerical approach was therefore adopted using a finite-element program developed at Imperial College.[16] Since this was completed, an experimental study of guided wave propagation in an immersed plate has been reported by Guillet *et al.*[17] Although the approach of his work was somewhat different, the conclusions generally agree with the findings given in this section.

A dynamic finite-element model employing tapering elements was used to model five cases of varying asymmetric taper (1:80, 1:40, 1:20, 1:10, 1:5), the use of tapering elements having been validated. (For further details of the tapered element validation, see [18].) The simplest approach was to use the designated skin thickness of 1.2

mm and the double-skin thickness of 2.4 mm and simply vary the length and the number of elements across the tapered region to suit the required gradient. Fig. 3 illustrates the model geometry, in which excitation displacements were applied to the nodes at the left-hand end. The lower surface displacements were monitored in both x and y directions at 64 nodes in the input region and a further 64 nodes were similarly monitored in the output region, as shown. These monitoring regions enabled processing of the results by the two-dimensional Fourier transform technique[19] in order to separate the modes. Reflection ratios were calculated from the relative amplitudes of the center-frequency components of input and reflected signals.

The relative reflection ratios from the various taper gradients were investigated for three different input modes: A_0 at 0.56 MHz, S_0 at 0.5 MHz and A_1 at 2.2 MHz (using a 20 cycle Hanning-windowed tone burst in each case). These modes were chosen to be points of low dispersion across the thick, input, and thin, output regions of the model. In Fig 2b) these mode points have been marked. Point (**a**) is the A_0 mode in the thin output region, while (**a**′) is the same mode in the thicker input region. (The frequency has been adjusted to take account of the change in frequency-thickness product.) Points (**b**), (**b**′) and (**c**), (**c**′) are similarly plotted for the S_0 and A_1 modes respectively. It is seen that the A_0 and A_1 modes are reasonably non-dispersive in both input and output regions, while the S_0 mode is quite dispersive in the input region (The long wavelength of S_0 at lower frequencies would have caused other problems). The possibility of interference of reflections from both the leading and trailing edges of the tapered region meant that a precise reflection coefficient for each mode could not be established. Table II indicates the out-of-plane amplitude reflection coefficient for the maximum signal reflected from the tapered region with respect to the input signal. Transmission ratios were also obtained by comparing the center frequency components of input and transmitted signals. However, the change of mode (owing to the change in skin thickness), implies a change in the mode shape, with the result that the transmission ratios are not a simple indication of the energy lost at the change in section and the transmission ratios are consequently omitted.

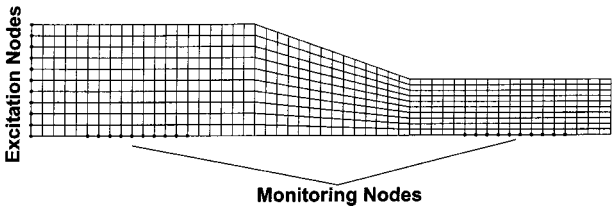

Fig. 3. Finite-element mesh used to model a region of tapering thickness.

Table II. Maximum reflection coefficient from the tapered region predicted by finite-element analysis considering out-of-plane displacements. Plate tapered in thickness from 2.4 mm at the input end to 1.2mm at the output end. Experimentally measured values for input A_0 are shown in brackets

Taper Gradient	Input Mode		
	S_0 at 0.5 MHz	A_0 at 0.56 MHz	A_1 at 2.2 MHz
1:80	0.003	0 (0)	0.005
1:40	0.008	0.005 (0.018)	0.016
1:20	0.020	0.008 (not measured)	0.027
1:10	0.034	0.027 (0.020)	0.064
1:5	0.048	0.030 (0.023)	0.104

To validate the finite-element analysis, a practical experiment along similar lines was undertaken. Test specimens were constructed by milling 2.4 mm thick sheets of aluminium alloy to the dimensions shown in Fig. 4, which also shows the experimental arrangement employed. As in the numerical tests, the length of the tapered region was adjusted to give gradients of 1:80, 1:40, 1:20, 1:10 and 1:5. A Hanning-windowed, twenty-cycle tone burst of the A_0 mode was generated by means of a signal generator driving a local immersion transducer [10] and both incident and reflected signals were received by means of a conical, point-contact transducer.[20] The received signals were sampled and displayed on a digital oscilloscope and were stored and processed on a personal computer. Parafin wax was used to form the local-immersion bath to absorb reflections that would otherwise reverberate in the water path. For each gradient, the maximum measured reflection from the tapered region is indicated, in brackets, in the column for A_0 in Table II.

Although the numerical and experimental results are not directly comparable, owing to differences in the interference of the reflections, it is clear that in both cases

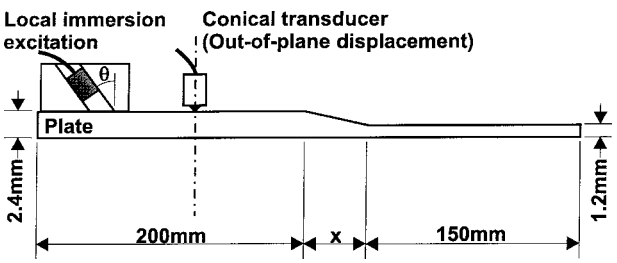

Fig. 4. Tapered skin experimental test specimen and equipment arrangement for tapered skin experiments.

the amplitudes of the reflections are small (<3%). Interference also obscures the trend but, as expected, the reflection amplitude increases with gradient. In general the finite-element results indicate that a reflection of less than 10% can be expected for gradients of up to 1:5. In most cases the reflection is insignificant.

6. SKIN LOADED WITH SEALANT

Guided waves in plates loaded with an inviscid fluid, in particular water, have been thoroughly studied since the work of Osborne and Hart.[21,22] Consider the propagation of a mode in a free plate as it passes into a region where the plate is loaded on one side by a fluid. Provided that the mode exhibits some out-of-plane displacement at the plate surface, energy is coupled to the overlying fluid layer. If the phase velocity of the mode in the plate is greater than the bulk wave velocity in the fluid, energy will leak from the plate, generating waves in the fluid that propagate away from the plate at an angle determined by Snell's law. This leakage of energy causes considerable attenuation of the plate mode. When the plate is loaded by a solid half-space, modes with phase velocities greater than that of the bulk shear wave in the half-space leak shear-wave energy, while modes with phase velocities greater than the bulk longitudinal wave velocity in the half-space leak both shear and longitudinal wave energy. If a non-viscous liquid layer is fairly thin and no longer constitutes a half-space, the leaked energy is reflected from the free fairly thin and no longer constitutes a half-space, the leaked energy is reflected from the free boundaries of the liquid layer back towards the plate. Energy no longer escapes the system and the reverberation between the free boundaries form modes propagating in the double-layer system. These modes have no attenuation mechanisms other than those identified for the free plate. When the fluid layer is viscous, however, these modes have significant attenuation owing to viscous losses in the fluid. Thus, two distinctly different types of propagation are possible in this system, dependent upon the thickness of the viscous layer. Since the PRC sealant (described in section 3) is highly attenuative, it was considered possible that even a relatively thin layer might effectively constitute a half-space. Thus it was necessary to determine which type of propagation was valid for the thickness of sealant that might be encountered in aircraft.

A comparison of the phase velocity and attenuation spectra for skins loaded with 1.4 mm thick layers of viscous and non-viscous sealant is shown in Fig. 5, where there is a marked difference in the phase velocity spectra. The non-viscous case supports many more modes than

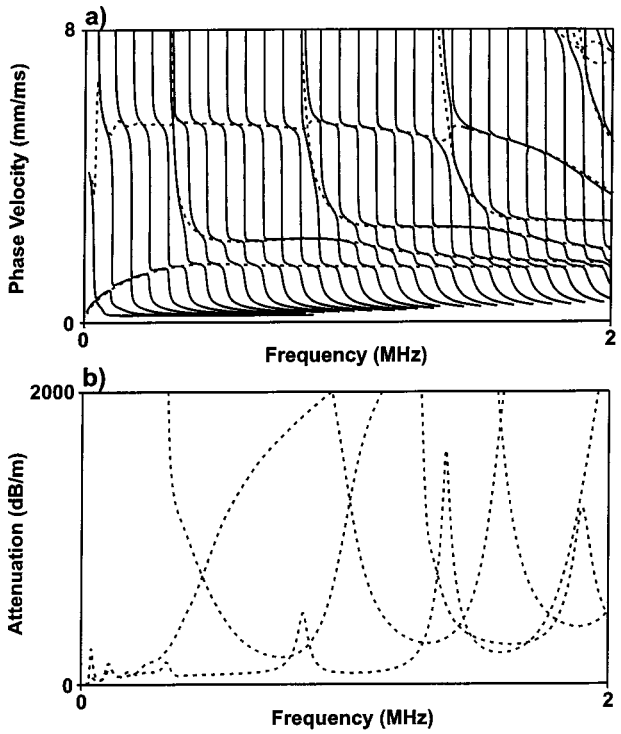

Fig. 5. a) Phase velocity and b) Attenuation spectra for the case of 1.2 mm thick skin loaded with a 1.4 mm thick layer of PRC sealant comparing viscous (- - - - -) and non-viscous (———) sealant. (Attenuation is zero in the non-viscous case.)

the viscous case, because the partial waves of these modes are not able to couple across a viscous layer of this thickness. There is, of course, a radical difference in attenuation: all the modes of the non-viscous case have zero attenuation, because there is no leakage from the system and no viscous loss.

During aircraft assembly the sealant is usually spread onto the surface by hand with a spatula or brush and there is a considerable variation in thickness. The effect of a 10% change in thickness of the sealant layer was also studied.[18] It was found that thickness changes only cause the phase velocity spectrum to be shifted in frequency, commensurate with the change in frequency-thickness product. Perhaps more surprisingly, a similar pattern was seen in the attenuation spectra, with little change in the minimum attenuation of each mode. In general, aircraft may have a sealant thickness of as much as 5 mm in places and the lowest attenuation in this case is roughly the same as that for much thinner layers of PRC. Generally the minimum attenuation increases with mode order, so that the lowest attenuation is found in the fundamental modes at low frequency. The effect of variation of the sealant parameters was investigated, but

this was found to have little effect on the overall minimum attenuation.

Having established the appropriate dispersion characteristics, it is seen that, with the exception of the two fundamental modes at low frequency, all of the modes in this system have alternative much greater than 40 dB/m. (This is not strictly so, since at much higher frequencies, some modes exist with little or no surface displacement at the sealant-aluminium interface. These modes include the Rayleigh wave on the unloaded surface and other modes coincident in phase velocity with the longitudinal bulk wave velocity in aluminium. However, these are not practically useful for long range propagation because the Rayleigh wave is subject to high attenuation by paint layers and would need to be excited on the external surface. The other modes would require access to a cross-sectional area of the skin for excitation and reception and would not propagate across lap joints.)

In an initial validation of the dispersion curves of this system the attenuation and group velocity of propagating modes were measured using the pitch-catch arrangement shown in Fig. 6, at values of x between 110 mm and 40 mm in increments of 10 mm. Sealant covered 98 mm of the plate at the end remote from the transmitter. Two modes at attenuation minima were chosen. At 0.75 MHz an S_0 mode was excited in the free plate region by setting the excitation transducer to an angle of 16° with respect to the plate normal, while at 0.98 MHz, using an excitation angle of 36°, an A_0 mode was launched. Fig. 7 shows the dispersion curves of the sealant region with the phase velocity spectra of the free plate fundamental modes superimposed. Mode **d** in Fig. 7 has a similar mode shape and phase velocity to the S_0 mode in the free plate, while modes **a**, **b**, and **c** have mode shapes and phase velocities more closely corresponding to those of A_0 in the free plate. Table III compares the predicted and measured attenuation for the modes indicated on the dispersion curves.

It is interesting to note that minima in the attenuation spectra closely correspond with points where the phase velocity coincides with that of a mode in the free plate system. These points define frequencies at which the ratio of strain energy density in the plate to that in the sealant

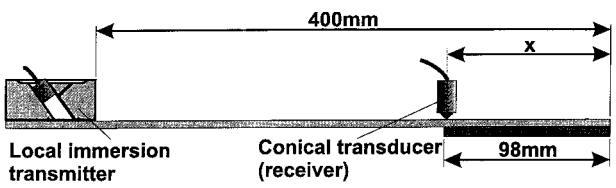

Fig. 6. Schematic diagram of the pitch/catch arrangement used to measure group velocity and attenuation in the sealant loaded system.

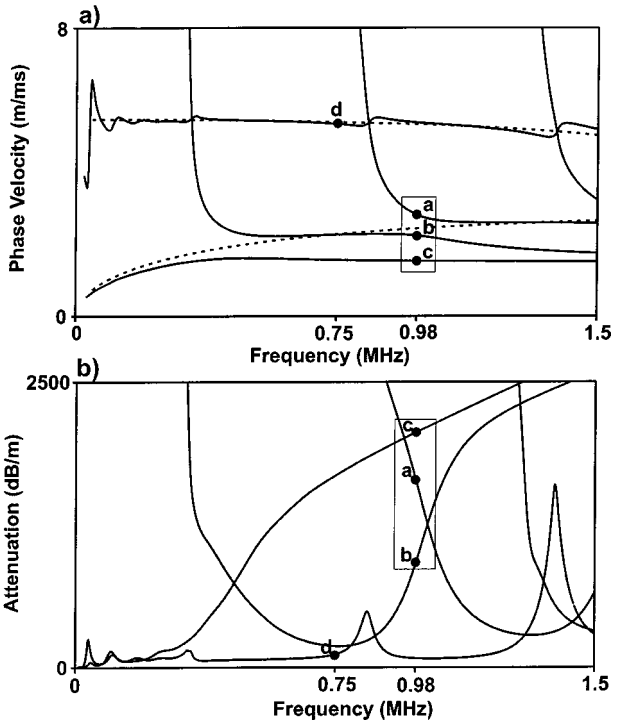

Fig. 7. a) Phase velocity and b) Attenuation spectra for the case of a 1.2 mm thick skin loaded with a 1.4 mm thick layer of PRC sealant compared with the corresponding spectra for the free plate case. Modes **a**, **b**, and **c** are strongly excited by an input A_0 signal at 1 MHz, while mode **d** is strongly generated by an input S_0 signal at 0.75 MHz.

layer is maximised. At such points, the mode shape within the plate section of the double-layer system most closely matches that of the corresponding mode in the free plate. This has important implications for the mode conversion. At the leading edge of the sealant layer all of the modes of the double-layer system existing at the excitation frequency are generated by mode conversion, but most of the input energy is transferred to modes with similar phase velocity and mode shape to those of the incident mode. Thus the S_0 mode is primarily converted to mode **d** and the measured attenuation consequently fell closest to that of this mode. The A_0 input mode would have been primarily converted to modes **a**, **b**, and **c** in Fig. 7.

Table III. Predicted and measured attenuation of modes shown in Fig. 7

Mode	Predicted Attn (dB/m)	Measured Attn (dB/m)
a	1433	—
b	1077	903
c	2085	—
d	122	61

However, modes, **a** and **c** have considerably higher attenuation and rapidly decay to insignificant amplitude over a very short distance. Mode **b** has the closest phase velocity and mode shape to that of the input mode, which corresponds with a minimum in the attenuation spectrum as mentioned above. The experimental measurements at 0.98 MHz therefore corresponded most closely with the parameters of this mode. This preferential excitation of certain modes is a feature of double skin systems where it is of more practical importance, as discussed below.

The high frequency-thickness dependence of attenuation close to the measured mode points means that small errors in the layer thickness or material specifications could account for the lower measured attenuation than that predicted. Further validation of the dispersion predictions for S_0 at low frequencies, using a laser interferometer (Polytech OFV 512) to measure in-plane displacements, produced much closer correlation, with a maximum error in both the phase velocity and attenuation of six percent over the frequency band 200–300kHz. Further details can be found in [18]. Measurement of S_0 in this low frequency band also confirmed experimentally that attenuation of less than 40 dB/m is not obtainable in this system.

7. PAINTED SKIN

Most aircraft finishes are either cellulose, acrylic, or epoxy[23] and a number of specimens were obtained painted with military specification paint schemes of epoxy and acrylic. The thickness of the coats ranged from 0.03 mm to 0.05 mm including a primer coat of roughly 0.02 mm. Bulk wave measurements using a 50 MHz probe indicated a longitudinal wave velocity of 2500–3000 m/s and, using a 6 MHz shear probe, a shear wave velocity of 500–1300 m/s across all samples. The approximate values reflect the variation in paint types and the difficulty in establishing accurate paint thickness measurements. The dispersion curves of this system are shown in Fig. 8, together with validation measurements that indicate that only the attenuation differs significantly from the free skin case. The group velocity measurements agreed very closely with the predictions and experimental measurements of the attenuation of the fundamental modes between 0.8 and 1.5 MHz, using laser equipment, showed good correspondence with predictions for A_0 (that of S_0 being too low to measure accurately). Fig. 8 b) is therefore considered a reasonable estimate of the attenuation of modes propagating through painted skin and it is seen that at frequencies below 1 MHz, the attenuation of the fundamental modes is less than 6 dB/m. Above 2 MHz

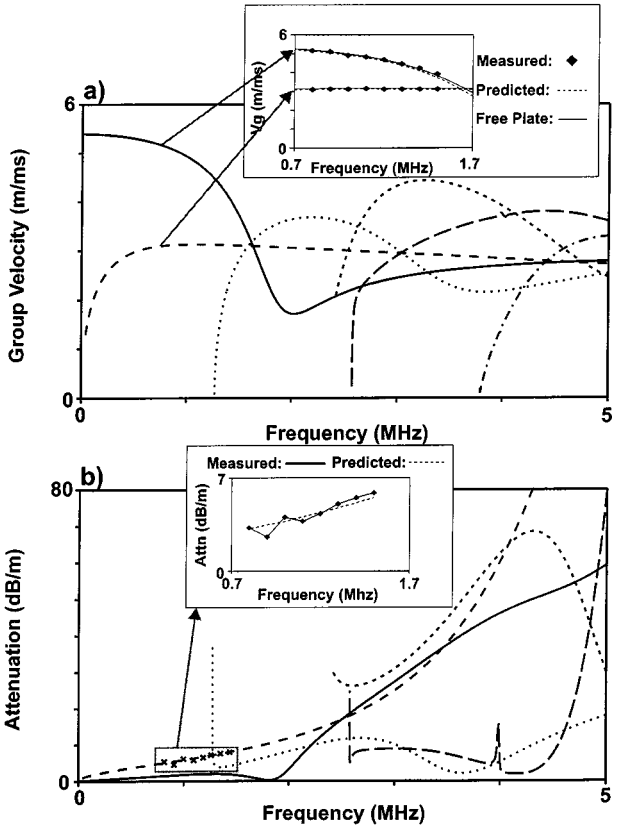

Fig. 8. a) Group velocity spectrum and b) attenuation spectrum for the paint loaded skin system. Measured values of group velocity and attenuation compared with dispersion predictions are shown in the insets for the modes indicated.

the attenuation of the fundamental modes rises sharply, tending, at high frequency, to that of a Rayleigh wave on each of the free paint surfaces (approximately 50 and 150 dB/m for the thin and thick paint surfaces respectively). The higher order modes generally have significant attenuation, with local minima where it falls to less than 6 dB/m. Thus the attenuation of paint layers should not be ignored at frequencies above about 2 MHz. This investigation also indicates that a Rayleigh wave on the external fuselage surface (assuming that it could be generated practically), would not be capable of long-range propagation.

8. PROPAGATION ACROSS DOUBLE SKIN SYSTEMS

Considerable research has been directed to examination of systems of joined aluminium skins, similar to those detailed here, and much of this work focused upon

propagation and defect detection in lap and stringer joints. Although some work deals more generally with propagation in the system, there is little interest in attenuation and long-range propagation. For example, Alers and Thompson[24] examined the related case of guided modes confined to the adhesive interlayer and identified modes sensitive to the interfacial properties of the joint and Mal *et al.*[25] found that for the bonded aluminium skin case, certain modes exhibit significant sensitivity to changes in bond stiffness.

The dispersion curves for PRC and Redux jointed double-skins, with respective jointing layer thicknesses of 0.3 and 0.25 mm, are presented in Fig. 9 and Fig. 10 respectively and the lower order modes are picked out using different line-types for clarity. An interesting feature of both systems is the 'twinning' of modes in the phase velocity spectrum. That is to say, pairs of modes with similar phase velocity over a broad frequency band are generally evident, particularly at lower frequencies. Typical pairs of modes are marked **a**,**b** and **c**,**d** in Fig. 9 and **e**,**f** and **g**,**h** in Fig. 10. The reason for this mode twinning is that, as was also seen in the previous section, the phase velocity is dominated by the elastic properties of the much stiffer and thicker aluminium skin layers. Just as was seen in the double layer system, each pair of

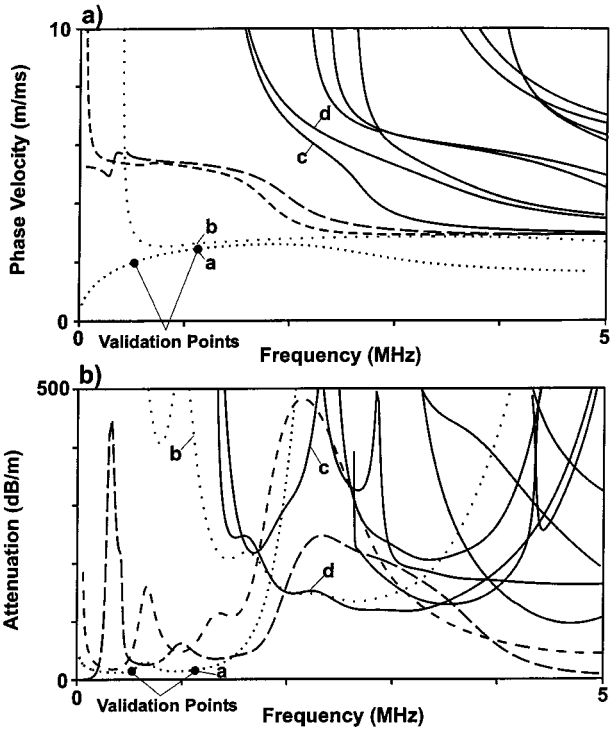

Fig. 9. Dispersion curves for system of two 1.2 mm skins jointed by a 0.3 mm PRC sealant interface layer. a) Phase velocity spectrum b) Attenuation spectrum.

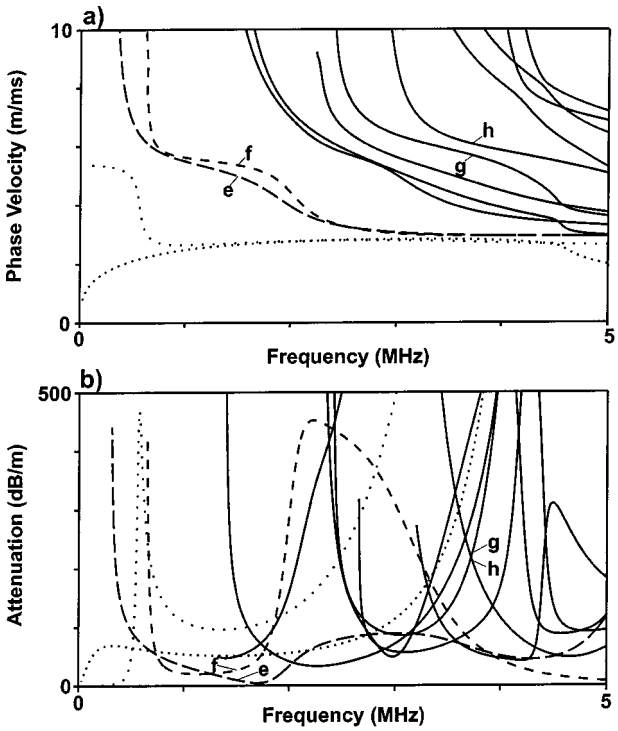

Fig. 10. Dispersion curves for system of two 1.2 mm skins jointed by a 0.25 mm Redux adhesive interface layer. a) Phase velocity spectrum b) Attenuation spectrum.

modes in the three-layer system will also exhibit a mode shape in the aluminium layers that resembles that of the corresponding mode of similar phase velocity in the free skin. The difference between the modes in a pair is a change of phase through the interface layer. This is illustrated in Fig. 11, which shows the mode shapes of the four pairs of modes indicated on Fig. 9 and Fig. 10. Thus, comparing the mode shapes in just the upper plates of any pair, they are found to be similar, but phase reversed. This will be seen to have important implications at the transition from single to double skin. The attenuation spectra of Fig. 9(b) and Fig. 10(b), though somewhat confusing, indicate that, except for certain bands, attenuation is generally greater than 40 dB/m.

Above about 2 MHz in the Redux bonded case and 1.5 MHz in the PRC jointed case, the attenuation of all but one mode is greater than 40 dB/m and this mode becomes the equivalent of a surface wave propagating on each of the free aluminium surfaces at high frequency. Hence, all of the potentially useful modes of these systems exist at frequencies below about 2 MHz. The problem is that the wavenumber proximity of twinned modes effectively prevents the excitation of just a single mode, irrespective of whether generation is by transduction on the joint region, or by mode conversion at the joint leading

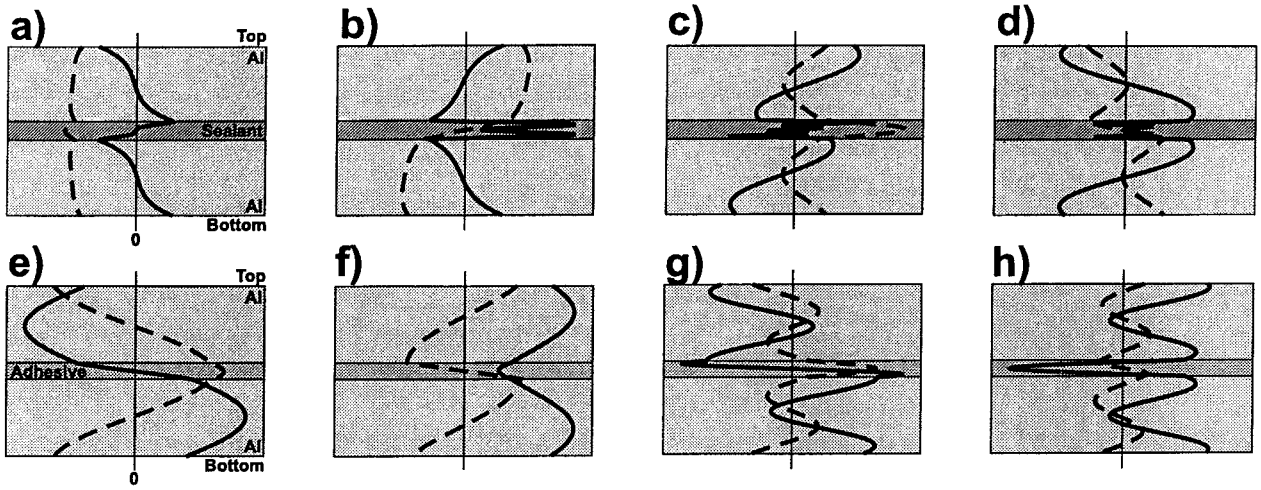

Fig. 11. Comparison of mode shapes of 'twinned' modes in double-layer systems. a), b), c) and d): mode shapes of double-skin system with sealant interface at points indicated in figure 9. e), f), g), and h): mode shapes of double-skin system with adhesive interface at points indicated in figure 10. (——— : In-plane displacement, - - - - - : Out-of-plane displacement.)

edge. In either case, the input energy is divided primarily between the pair of twinned modes. Examination of the dispersion curves of Fig. 9 and Fig. 10 reveals that, at some frequencies, one of the two twinned modes has a much higher attenuation. In this instance the amplitude of one mode will rapidly decay to insignificance, leaving the more gradual decay of the second mode over a greater distance. This may usefully reduce the effective number of propagating modes; nevertheless, a large proportion of the input energy is lost and, in the case of successive joints, this constitutes a further important attenuation mechanism. At frequencies where both of the twinned modes have a similarly low attenuation, they will propagate together over a considerable distance. In this instance, owing to the small difference between the phase velocities of the two modes, 'beating' occurs between the pair until they eventually become temporally and spatially separated. In joints where the propagation distance is relatively short, this interference mechanism dominates the efficiency of transmission, as discussed below.

8.1 Validation of Double-Skin System Dispersion Curves

The difficulty in obtaining single mode propagation of a non-dispersive mode, with reasonable attenuation, made validation of the dispersion curves of the double-skin systems very difficult. Techniques such as the two-dimensional Fourier transform[19] cannot be used to separate the interfering twinned modes because they have very similar wavenumbers. Nevertheless, in some of the experiments made on PRC joints, using an A_0 input mode, the attenuation of one of the twinned pair was very much greater than the other. After sufficient propagation in a broad joint, the amplitude of one mode had decayed to insignificance, allowing a rough measurement to be made of the group velocity and continuing attenuation of the other. These points are marked on the dispersion curves of Fig. 9 and the measurements are presented in Table IV, where group velocity shows much closer agreement with the predictions than attenuation, reflecting the fact that attenuation is much more difficult to measure accurately. At these comparatively low values of attenuation, reasonable errors in the attenuation measurements have resulted in large percentage errors, particularly for the A_0 mode at 1.1 MHz. The agreement between the predicted and measured attenuation was, nevertheless, sufficient to confirm the acquired mode.

9. PROPAGATION ACROSS AIRCRAFT JOINTS

Two types of joint: the lap joint and the stringer joint, described in the introductory text and illustrated in Fig. 1, were considered. Whilst the lap joint is found at the boundaries of fuselage skin plates, the stringer joint, which represents the point of attachment of support structure to the skin, occurs at regular intervals of about 100 mm along the fuselage longitudinal axis. Waves propagating through the skin would therefore be expected to encounter a high density of stringer joints. The interaction of guided waves with such discontinuous systems cannot

Table IV. Measured and predicted points on dispersion curves of double-skin system with 0.3 mm PRC interlayer. Refer to Fig. 9

	Attenuation (dB/m)		Group Velocity (m/ms)	
Input Mode	Experiment Theory	Error	Experiment Theory	Error
A_0 at 0.54 MHz	14.77	12.8%	2.92	2.6%
	16.94		2.99	
A_0 at 1.1 MHz	23.28	56%	3.08	0.2%
	14.94		3.09	

be adequately analysed by dispersion curves alone. Some analytical study of joints with idealised geometry have been reported, where no interface (or jointing) layer was included and limiting boundary conditions of either slip or no-slip at the interface were imposed.[26,27] In general, however, difficulty in satisfying the boundary conditions on all the surfaces within the joint precludes any closed-form solution for practical cases. In such cases numerical techniques are utilised. Chang *et al.*[28] and Mal *et al.*[29] studied the case of a lap joint with no jointing layer using a hybrid finite-element technique. Since Rokhlin outlined the potential of Lamb waves for adhesive bond inspection, many workers have concerned themselves with the detection of joint defects from guided wave interaction with joints. Pilarski *et al.*[30] proposed a mode selection criterion for the detection of interfacial weakness, based upon the multiplication of surface out-of-plane displacement and power, integrated over the region close to the interface and Challis *et al.*[31] showed that bond dimensions could be derived from transmitted Lamb wave signals by careful signal processing. Considerable experimental work, directly concerned with aircraft joints, has been undertaken by Sun and Johnston,[32–34] with the aim of detecting delamination and corrosion in aircraft joints; some of this work even includes riveted joints.[35] Much of the research mentioned above showed encouraging results. However, despite the suggestion by Rose *et al.*,[36] that the long-range characteristics and variety of mode shapes offered by guided waves may be exploited to improve the inspection efficiency of bonded joints, little attention was paid to the mutual interaction of modes propagating in the jointed region. This has important and far-reaching consequences for the transmission across joints, as will be seen, and such interaction will undoubtedly influence the results of defect detection in the bonded region. More recently a numerical study by Lowe and co-workers examined the generation and interaction of modes in the joint region, for the estimation of bondline thickness.[37]

9.1 Carrier Modes

Consider the interaction of a mode propagating in a single skin with the leading edge of a joint. Fig. 12 illustrates schematically an example of such an interaction, when the S_0 mode, propagating in the skin, encounters a lap joint with a 0.3 mm thick sealant interlayer. The leading edge area of the joint is depicted in cross-section by a light broken line, and the mode shape of the S_0 input mode is superimposed on the single-skin region. The change in section at the joint leading edge marks a step change in the elastic and geometric properties of the waveguide, which forces mode conversion of the input mode. Since the geometric change is asymmetric, the input mode may be mode converted to any, or all, of the possible modes that can exist within the bandwidth of the input signal. In principle, all of the possible modes will be generated with differing amplitudes, such that the boundary conditions are satisfied. In fact, the more similar the mode-shape of a possible propagating mode in the joint to that of the input mode, the more strongly it is likely to be generated by mode conversion. This is consistent with the 'Normal Mode Theory' discussed by Auld[38] and has been found to apply strongly to joint systems such as these.[37]

The double-skinned region of the joint with a 0.3 mm- thick sealant jointing layer was a system introduced in section 8. As was found generally in the multi-layered systems, the S_0 input signal will be predominantly mode-converted to the pair of modes with similar phase velocity and mode shape to those of the input S_0 mode. These modes carry most of the energy of the incident mode

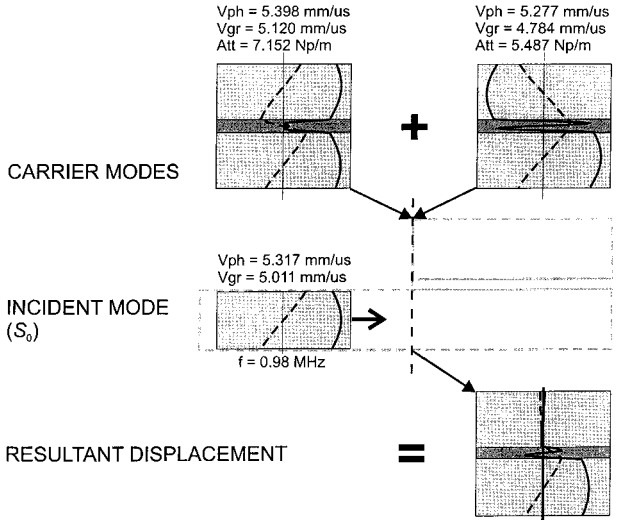

Fig. 12. Schematic diagram of carrier-mode interference at the leading edge of a joint (- - - - - : Out-of-plane displacement, ——— : In-plane displacement.)

across the joint and are termed ‘carrier modes’. The mode shapes of the two principal carrier modes for input S_0 at 0.98 MHz can be seen above the joint in Fig. 12. For each of these mode shapes, consider just the lower section, which represents the lower plate in the bonded region. It is clear that the mode shapes in the lower plate are very similar and closely resemble that of the input mode in the single-skin region. Both modes are therefore very strongly generated by mode-conversion at the leading edge. In section 8 it was mentioned that the essential difference between a pair of twinned modes is an extra phase change in the interface layer. This is seen in both the in-plane and out-of-plane displacements in the carrier mode shapes in Fig. 12. In the upper plate, the mode shapes of the carrier modes are once again similar, but are in phase opposition owing to the phase change. When the two carrier modes are generated by mode-conversion at the leading edge, they are superimposed and the resulting displacement, which is the sum of the two mode shapes, is shown below the joint. The resultant shows that in the lower plate the displacements of the carrier modes sum constructively, while in the upper plate the displacements are largely destructive. There is consequently very little surface displacement amplitude at the joint leading edge.

Perfect cancellation at the leading edge does not occur. Firstly, this is because the carrier mode shapes in the upper plate are not perfect, phase-reversed, copies of each other. Secondly, the diagram in Fig. 12 is schematic and in reality other modes within the bandwidth of the input signal are also excited to some extent, and the amplitudes of the principal carrier modes may not be exactly equal as implied by the figure. Finally, the numerical analysis, presented shortly, found that a surface wave is generated on the vertical leading edge of the upper plate, and this also contributes some surface displacement at the leading edge.

Once generated, the two principal carrier modes propagate away from the leading edge with similar, but not equal, phase velocity. This difference in phase velocity results in a cyclic change in the resultant displacement as the modes propagate temporally and spatially through the double-skin region. The carrier modes are effectively ‘beating’ together, and the displacement amplitude on the surface of the upper plate in Fig. 12 changes cyclically between a destructive and constructive interference condition at spatial intervals along the plate surface, the opposite condition being found at corresponding positions on the lower plate. A similar ‘beating’ is found in a free plate at high frequency-thickness products, where the two fundamental modes, having very similar phase velocities, form what is usually termed the pseudo-Rayleigh wave. This mutual interaction is discussed by Auld[38] who describes a coupling of the two modes across the plate, with energy being transferred in a temporal and spatial cyclic pattern from one surface of the plate to the other, over a spatial distance that he calls the ‘coupling length’. As one might expect, increasing the carrier-mode phase velocity difference shortens the coupling length. Indeed, the coupling length (S_c) is simply related to the difference in wavenumber of the two carrier modes (k_1 and k_2) such that:

$$S_c = \frac{\pi}{|k_1 - k_2|} \tag{1}$$

Where signals of finite length are employed, as is invariably the case in NDE, the carrier-mode signals will eventually separate, given a sufficiently long propagation distance. In some cases, one of the principal carrier modes has a much greater attenuation and its influence rapidly diminishes with distance from the leading edge, leaving just the decay of the other mode. Bonded joints exhibit the same carrier-mode generation and interference, since the dispersion curves, presented in Fig. 10, show similar mode twinning in the phase velocity spectrum.

9.2 Experiments

To illuminate the carrier-mode generation and interaction within the joint and to support the numerical analysis described below, experimental work compared the interference pattern appearing over the surface of the joints with that predicted by dynamic finite-element analysis. Since frequency domain methods are not able to separate modes of similar wavenumber, the results were generally processed in the time domain by measuring the parameters of the interference pattern, particularly the ‘coupling length’. Employing the signal generator and local-immersion transmitter described in section 5 above, Fig. 13 illustrates an example of the experimental arrangement. A laser receiver was used to measure the out-of-plane surface displacements across the specimen, at intervals of 10 mm from the leading edge denoted by *d*. In some earlier experiments a local-immersion receiver, identical to the transmitter, was used. The time domain

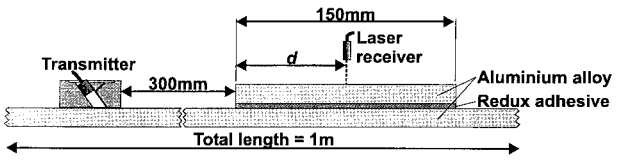

Fig. 13. Experimental arrangement used to examine the interference pattern across specimen D. (Refer to tables 5 and 6).

Table V. Experimental specimens

ID	Jointing Material	Type	Jointed Length (mm)	Bond thickness (mm)
B	PRC	Lap	150	0.3 ± 6%
C	Redux	Lap	150	0.25 ± 4%
D	Redux	Stringer	150	0.26 ± 2%

signal at each measurement point on the surface of the overlap region of the joint specimens specified in Table V, was sampled by a digital oscilloscope and processed on a PC. All the joint specimens featured a 150 mm overlap in order to avoid the interference of signals reverberating over the length of the overlap region. Table 6 lists the modes examined, together with the specimen used in each case. This table also indicates the phase velocities (V_1, V_2) of the two carrier modes and their respective attenuations (α_1, α_2) derived from the dispersion predictions. The coupling length (S_c), defined in the equation above, is also shown. The first experiments examined the four modes in the sealant jointed specimen (B in Table V) and, having observed the interference of the modes, subsequent experiments and modelling concentrated on just the S_0 mode in the frequency band between 1 MHz and 1.5 MHz. In this band an almost linear divergence in the relative phase velocity of the carrier modes is seen in Fig. 9 and Fig. 10.

The maximum amplitude of the signal envelope received at each location was established using the well-known Hilbert transform technique.[39] This amplitude was plotted against the distance from the joint leading edge, and the results were compared with the calculated coupling length and subsequently with those of equivalent numerical modelling exercises.

9.3 Numerical Modelling

Using the finite-element software employed for tapered skin modelling, a study was carried out to reveal more clearly the interference across the thickness of the bonded region and to examine more closely events at the joint leading edge. An important limitation of the modelling software in this case was that it did not accommodate material damping. Furthermore, to avoid model instability the maximum mesh size is determined from the velocity of the slowest wave within the signal bandwidth and the maximum time step is subsequently determined by the velocity of the fastest wave as described by Blake.[40] Owing to the very large difference between the bulk longitudinal wave velocity in the aluminium alloy skin and the bulk shear wave velocity in the PRC sealant, it was not possible to model systems with PRC sealant layers.

9.4 Results

9.4.1 Joint with a Sealant Interlayer

Fig. 14 a) illustrates an example of the results of the experiments on the lap joint with a sealant interface (specimen B), showing the signals received by local-immersion transducers at spatial intervals across the free surface of the output plate in the overlap region. These are presented in the form of a 'waterfall' plot that highlights the differences between the signals at each location. For each time trace in the waterfall plots, the time axis originates at the centre (maximum amplitude) of the input tone burst. The amplitude of the signal is seen to be increasing with distance from the leading edge reaching a maximum at about 80 mm. Fig. 14 b) plots the respective maximum amplitudes of the signals in Fig. 14 a) by means

Table VI. Details of experimentally examined modes

Input Mode	Frequency (MHz)	Jointing Material	Type	Specimen	Predicted Parameters				
					Phase velocity V_1 (m/s)	Phase velocity V_2 (m/s)	Attenuation α_1 (dB/m)	Attenuation α_2 (dB/m)	Coupling length S_0 (mm)
S_0	0.98	PRC	Lap	B	5371	5244	54	43	113
A_0	0.55	PRC	Lap	B	2787	2088	758	21	8
A_0	1.1	PRC	Lap	B	2662	2482	366	15	18
S_0	1.1	Redux	Lap	C	5557	5381	20	29	77
S_0	1.55	Redux	Lap	C	5309	4894	26	8	20
A_1	2.27	Redux	Lap	C	6369	6138	33	357	37
S_0	1.1	Redux	Stringer	D	5557	5381	20	29	77
S_0	1.5	Redux	Stringer	D	5309	4894	26	8	20
A_0	1.1	Redux	Stringer	D	2646	2523	103	53	25

of a broken line. In addition, the corresponding results from later laser experiments are superimposed, using a solid line. The data in each series has been independently normalised by dividing by the mean of the amplitudes of the data points in the range common to both laser and local-immersion experiments. It is seen that the local-immersion and laser results are in close agreement, particularly in respect of the period of the amplitude fluctuation. The coupling length of the carrier modes of S_0 at 0.98 MHz is seen in Table VI to be 113 mm, but the maximum amplitude in Fig. 14 occurs at only 80 mm from the joint leading edge. However, just a 0.5% error in the phase velocity of one of the carrier modes would account for this disagreement and such an error is likely, given the variation in the PRC properties.

Except for the initial rise in amplitude close to the leading edge, the interference pattern produced by the two principal carriers was not generally seen in the experiments on sealant jointed specimens, owing to the high attenuation of one mode. This was not the case however, for the bonded joints, considered next.

9.4.2 Joints with an Adhesive Interlayer

The waterfall plots of Fig. 15 a) and b) show received signals for the case where the input mode to the bonded lap joint was S_0 at 1.5 MHz. In this case a 50 cycle Hanning-windowed tone was employed to avoid dispersion. Fig. 15 a) shows the waterfall plot for the bonded region of the upper surface of the output plate, while Fig. 15 b) shows the corresponding plot for the lower surface of the input plate in the bonded region. In both figures the interference pattern is clearly seen. Comparing corresponding locations on the two figures one finds that positions where the envelope amplitude is greatest in one figure correspond with minimum envelope amplitude in the other. Thus, the swapping of energy from one side of the system to the other, with propagation distance was observed. In this case the predicted attenuation of the carrier modes was 8 dB/m and 26 dB/m, both of which are relatively low and so the interference pattern extends across the whole joint.

To illustrate the dependence of coupling length on the difference in the carrier-mode phase velocities, the variation of maximum surface amplitude for an input S_0

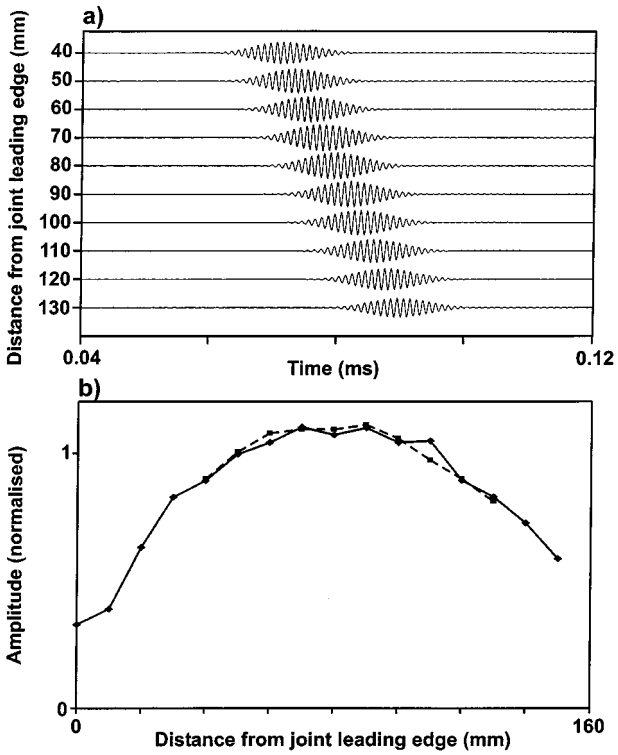

Fig. 14. Example of experimental results obtained from the sealant jointed lap joint presented a) in the form a 'waterfall' plot b) a surface amplitude plot for the input mode: S_0 at 0.98 MHz (——— laser receiver measurements, - - - - - local-immersion receiver measurements).

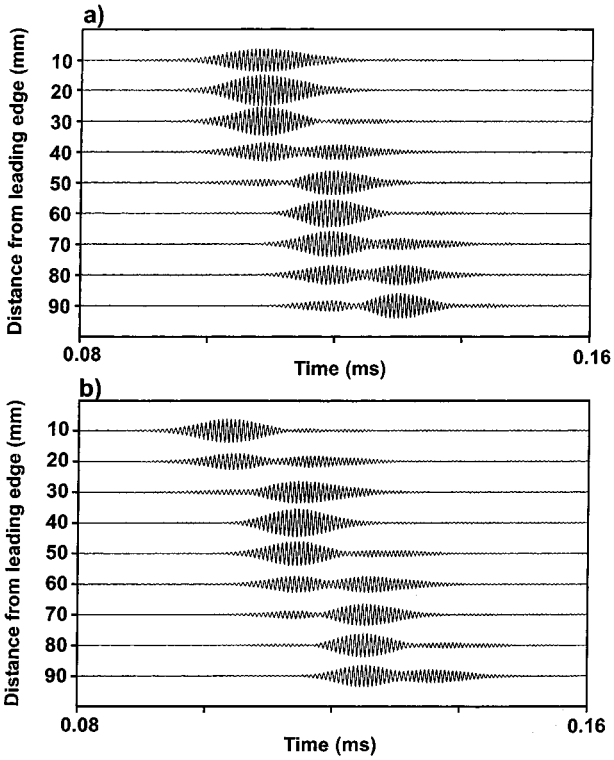

Fig. 15. Experimental results obtained from the bonded lap joint, presented in the form of 'waterfall' plots for points across the surface of a) the upper (output) plate and b) the lower (input) plate for an input mode of S_0 at 1.5 MHz.

mode at 1.1 MHz and 1.5 MHz are shown in Fig. 16 a) and b) respectively. Corresponding results from the numerical analysis are superimposed and show good agreement in both cases, particularly with respect to the period of cyclic variation. From Table 6, the coupling distance for input S_0 at 1.1 MHz is seen to be 77 mm. The period of amplitude variation in Fig. 16 a), however, is about 120 mm, implying a coupling length of only 60 mm. This error is likely to have been caused by small inaccuracies in thickness or adhesive properties assumed in the prediction, but joint reverberation, and perhaps also the presence of low amplitude modes other than the S_0 primary carriers, could have been contributory factors.

Table 6 indicates that at 1.5 MHz the coupling length for input S_0 reduces to 20 mm, owing to the increased relative difference in the carrier-mode phase velocities at this frequency. Fig. 16 b) shows a cyclic amplitude variation with a period of about 40 mm, indicating a coupling length of 20 mm that corresponds with the predicted value. As expected, the pattern on the opposite surface of the jointed area showed a similar variation with an opposite phase. The experimental results for the stringer joint were very similar, though the different thickness of the adhesive layer resulted in differences in the coupling lengths compared with the lap joint.

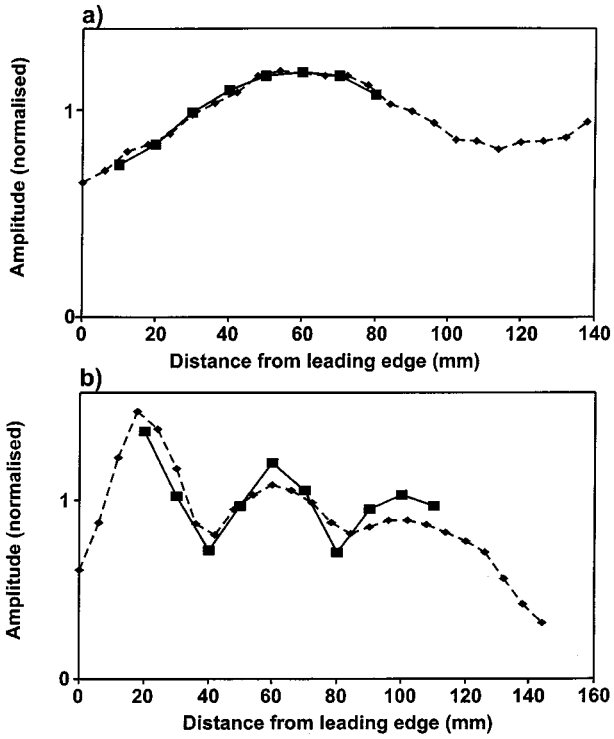

Fig. 16. Graphs of surface amplitude for locations on the free surface of the output plate in the overlap region of the bonded lap joint for the cases of an S_0 input mode at: a) 1.1 MHz and b) 1.5 MHz. (——— : experimental results, - - - - - : numerical predictions. Results are independently normalised by dividing by the mean of the amplitude of points in the range common to both data sets.)

This interference pattern is very important, since it was found in the experiments, and in the modelling of whole joints, that it largely determined the efficiency of propagation across the joint. Optimum transmission will occur when the carrier-mode interference results in maximum amplitude in the output plate at the trailing edge of the joint. This mechanism is graphically illustrated in Fig. 17, which shows a snapshot in time from the full mesh output of the FE model for the case of an S_0 mode, input to a bonded lap joint at a frequency of 1.5 MHz. The input mode is a twenty-cycle tone burst, so that the situation shown in the figure approximates the steady state condition. In order to see clearly the interference pattern in the jointed region only a small section of the mesh in the region of the joint is shown in the figure. At the leading edge of the joint there is very little amplitude on the surface of the output plate and large amplitude on the input plate surface below. This situation is the equivalent of that illustrated in Fig. 12 (for the sealant joint). By the time the trailing edge of the joint is reached, the interference condition is reversed and a large amplitude is now seen on the output plate surface with very little amplitude on the corresponding input plate surface. Excellent transmission into the output plate is clearly seen and it is also apparent that there is very little reflection from the end of the input plate at the trailing edge. The latter is equally important, since it results in less joint reverberation.

Finally, as a practical illustration of these results, Fig. 18 presents two time-domain traces from a simple pulse-echo experiment. Once again, this example shows the case of the S_0 mode input to the bonded lap joint shown above the graphs. Fig. 18 a) shows the worst transmission case at 1 MHz. In this graph a large reflec-

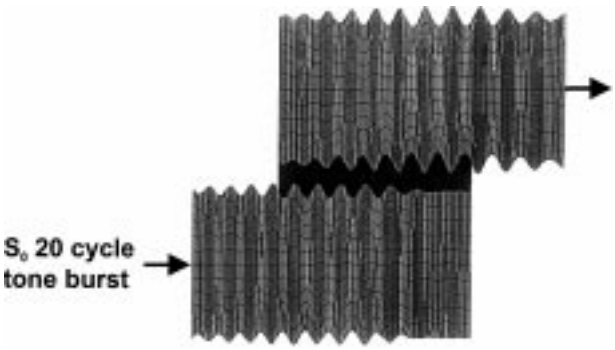

Fig. 17. View of the entire mesh of a finite-element model of a bonded lap joint, showing excellent transmission of a 20 cycle input tone burst of the S_0 mode at 1.5 MHz.

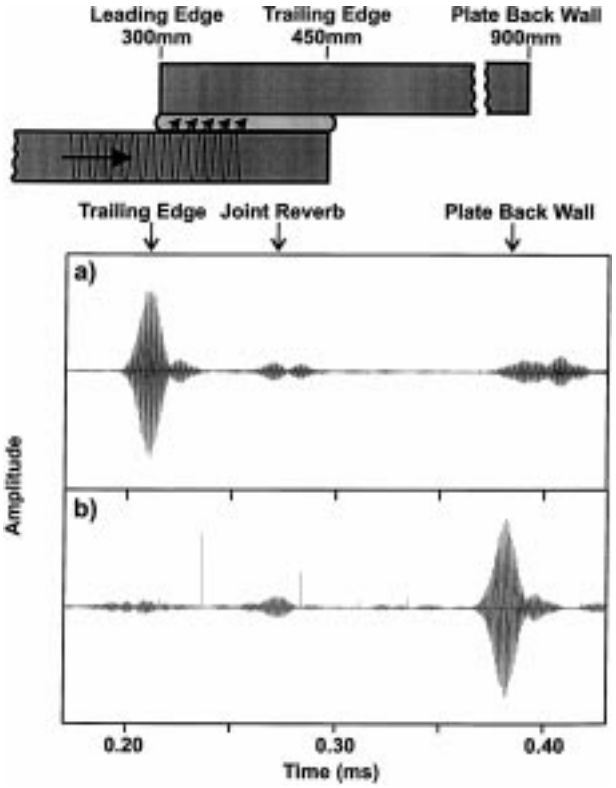

Fig. 18. Results of a pulse-echo experiment showing: a) worst transmission across an adhesive lap joint at 1 MHz and b) optimum transmission at 1.5 MHz.

tion from the trailing edge of the joint is indicated in the figure. This is followed by some joint reverberation, after which a small reflection from the back wall of the output plate is seen, indicating poor transmission across the joint. Simply changing the input frequency to 1.5 MHz results in the optimum transmission case shown in Fig. 18 b). Here the reflection from the joint trailing edge has very much diminished in amplitude, while the reflection from the output plate back wall is significantly larger. This optimum transmission case is particularly encouraging when one considers that, since this is a pulse-echo experiment, the signal has traversed the 150 mm-wide bonded region twice. The same test, applied to the stringer joint specimen, found that although optimum transmission occurred at a frequency of 1.08 MHz, similar to the worst transmission frequency in the lap joint as expected, the best transmission frequency was not 1.5 MHz, but 1.2 MHz. This difference is consistent with differences in the bond thickness and material parameters of the two joints. The effect of such variations would be more apparent when, as in this case, the coupling length is short. Indeed, this problem with the short coupling length highlights a crucial problem that arises when transmission is attempted across a series of narrow joints.

Although these results are most encouraging in respect of a single joint, similar results were not obtainable from a series of joints, such as is presented by a succession of bonded fuselage stringers. A typical stringer joint is about 20 mm in width and optimum transmission is obtained only if the first constructive maximum occurs in the output plate at the joint trailing edge. In this case the optimum coupling length is only 10 mm. With such a short coupling length, small variations in the joint dimensions (and perhaps also adhesive properties) cause radical departure from optimum transmission across successive joints. This results in a cumulative degradation of the transmission efficiency over a series of joints. A number of practical laboratory tests were carried out on a specimen with several bonded stringers spaced at intervals of 100 mm. Transmission across more than four stringers with an effective attenuation of less than 40 dB/m was unobtainable when twinned carrier modes were present in the bonded regions, even though transmission across the first joint was about 90% efficient. At the time, this finding was somewhat perplexing, since commercial acoustic emission systems receive signals that have propagated over several meters through metallic fuselage structure. Such signals can only be guided-wave modes. Subsequent investigation of this issue [18] found that AE signal energy is primarily confined to low frequency bands where mode twinning does not occur. These low-frequency fundamental modes are of little use in an active system, because the long wavelength of the S_0 mode gives poor spatial resolution of structural features and the A_0 mode is highly dispersive. There is insufficient space here to present the details of this work, which will be covered in another paper.[41]

10. CONCLUSIONS

The complexity of metallic aircraft structure presents a serious problem for long range guided wave propagation, since no mode was found that could negotiate each of these simplified structural features with sufficiently low attenuation and at appropriate wavelength. Although long range propagation through simple and tapered skin presents little problem, as long as dispersion is avoided, overlying sealant layers were seen to cause a severe damping problem. Where sealant layers are greater than about 1 mm thick, all modes have attenuation greater than 40dB/m. The work presented has also demonstrated the problem of frequency-thickness sensitivity when transmitting guided waves across aircraft skin joints, owing to the

generation and interference of twinned carrier modes. Two possible situations arise: if one of the principal carrier modes has a much higher attenuation than the other, its amplitude decays to insignificance over a very short distance in the joint, leaving the less attenuative mode. Where both principal carrier modes exhibit low attenuation, beating occurs over a considerable distance across the joint, resulting in a clear pattern of surface displacement. The cyclic period of this pattern can be estimated from the relative wavenumber of the carrier modes. For either a lap or a stringer joint, excellent transmission is achieved by arranging for constructive carrier-mode interference in the output plate at the joint trailing edge. This condition also results in less joint reverberation. Conversely, destructive interference in the output plate at the trailing edge results in the poorest transmission. More importantly, although excellent transmission across a single joint can be arranged, this was not found to be sustainable across a succession of narrow joints, such as are found in aircraft fuselage structure. In practice, the geometries of the structural features are likely to vary considerably and systems with more than two skin layers would be encountered. Fasteners, neglected here, would also add a difficult scattering problem.[42] Consequently, an integrated, single mode, active system, employing current transducer technology to monitor an entire fuselage is not feasible. However, guided waves do offer good potential for localised monitoring of structurally significant areas where a higher transducer density can be employed.

ACKNOWLEDGMENTS

This work was supported by the United Kingdom Department of Trade and Industry (DTI) and administered by the Defence Evaluation and Research Agency (DERA). The authors would like to acknowledge the assistance of B. Pavlakovic for the development of the program: 'Disperse', and D. Hitchings for the development of the numerical modelling program: 'Finel'. We are also indebted to D. Haddock for the provision of aircraft paint scheme samples.

REFERENCES

1. NTSB 'Aviation Accident Report', NTSB\AAR-89/03, National Transport Safety Board, Washington USA, 1989.
2. J. M. Carlyle, 'Acoustic Emission Testing The F111', *NDT international*, **22**(2):67–73, 1989.
3. M. R. Gorman, 'Plate wave acoustic emission', *Journal of the Acoustical Society of America*, **90**:358–364, 1991.
4. W. B. Spillman, 'Sensing and processing for smart structures', *Proceedings of the IEEE*, **84**(1):68–77, 1996.
5. B. Culshaw, 'Smart structures activities worldwide', *Proceedings of SPIE*, **2717**(2):3–17, 1996.
6. J. N. Kudva, C. Marantidis, and J. Gentry, 'Smart structures concepts for aircraft structural health monitoring', *Smart structures and intelligent systems SPIE*, **1917**:964–971, 1993.
7. D. Alleyne, M. Lowe, and P. Cawley, 'The inspection of chemical plant pipework using Lamb waves: defect sensitivity and field experience', In: Annual review of progress in quantitative NDE, Thompson DO, Chimenti DE eds., New York, Plenum Press, **15**:1859–1866, 1996.
8. T. H. G. Megson, '*Aircraft structures for engineering students*', Edward Arnold, London, 1990 2nd ed.
9. B. Pavlakovic, M. Lowe, D. Alleyne, and P. Cawley, 'Disperse: a general purpose program for creating dispersion curves', In: Annual review of progress in quantitative NDE, Thompson DO, Chimenti DE eds., New York, Plenum Press, **16**:155–192, 1997.
10. D. N. Alleyne, and P. Cawley, 'The interaction of Lamb waves with defects', *IEEE transactions on ultrasonics, ferroelectics, and frequency control*, **39**(3):381–397, 1992.
11. S. Rokhlin, 'Resonance phenomena of Lamb waves scattering by a finite crack in a solid layer', *Journal of the American Ceramic Society*, **69**(4):922–928, 1981.
12. Y. Cho, D. D. Hongerholt, and J. L. Rose, 'Lamb Wave scattering analysis for reflector characterization', *IEEE transactions on ultrasonics, ferroelectics, and frequency control*, **44**(1):44–51, 1997.
13. P. D. Wilcox, R. P. Dalton, M. J. S. Lowe, and P. Cawley, 'Mode and transducer selection for long range Lamb wave inspection', In: Key Engineering Materials, Gilchrist MD, Dulieu-Barton JM, Worden K. eds., Aedermannsdorf, Trans Tech, **167–168**:152–161, 1999.
14. D. N. Alleyne, and P. Cawley, 'Optimization of Lamb wave inspection techniques', *NDT and E international*, **25**:11–22, 1992.
15. P. M. Morse,'*Vibration and sound*', McGraw Hill, New York, 1948.
16. D. Hitchings, 'FE77 user manual', Imperial College, London, 1995.
17. A. Guillet, M. Kettani, and F. Luppe, 'Guided waves' propagation in an elastic plate of linearly varying thickness', *Journal of the Acoustical Society of America*, **105**(2):1340, 1999.
18. R. P. Dalton, 'Propagation of Lamb Waves through metallic aircraft fuselage structure', PhD thesis, Mechanical Engineering, Imperial College of Science, Technology and Medicine, 2000.
19. D. Alleyne, and P. Cawley, 'A two-dimensional Fourier transform method for the measurement of propagating multimode signals', *Journal of the Acoustical Society of America*, **89**(3):1159–1168, 1991.
20. M. J. Evans, 'Design of a self-calibrating simulated acoustic emission source', *Ultrasonics*, **37**:589–594, 2000.
21. M. Osborne, and S. Hart, 'Transmission, reflection, and guiding of an exponential pulse by a steel plate in water 1. Theory', *Journal of the Acoustical Society of America*, **17**(1):1–18, 1945.
22. M. Osborne, and S. Hart, 'Transmission, reflection, and guiding of an exponential pulse by a steel plate in water 2. Experiment', *Journal of the Acoustical Society of America*, **18**(1):170–184, 1946.
23. FAA '*Federal Aviation Administration—airframe handbook*', US Department of Transportation, Washington, 1976 2nd ed.
24. G. A. Alers, and R. B. Thompson, 'Application of trapped modes in layered media to the testing of adhesive bonds', *IEEE Ultrasonics Symposium*, 1976, Annapolis, MD, pp. 138–143.
25. A. K. Mal, P. C. Xu, and Y. Bar-Cohen, 'Analysis of leaky Lamb waves in bonded plates', *International journal of engineering science*, **27**(7):779–791, 1989.
26. S. Rokhlin, and F. Bendec, 'Coupling of Lamb waves with the aperture between two elastic sheets', *Journal of the American Ceramic Society*, **73**(1):55–60, 1983.
27. S. I. Rokhlin, 'Lamb wave interaction with lap-shear adhesive joints: theory and experiment', *Journal of the Acoustical Society of America*, **89**(6):2758–2765, 1991.

28. Z. Chang, D. Guo, and A. K. Mal, 'Lamb Wave Propagation across a Lap Joint', In: Annual review of progress in quantitative NDE, Thompson DO, Chimenti DE eds., New York, Plenum Press, **15**:185–191, 1996.
29. A. Mal, Z. Chang, D. Guo, and M. Gorman, 'Lap joint inspection using plate waves', *Proceedings of SPIE*, **2945**:128–137, 1996.
30. A. Pilarski, J. L. Rose, J. Ditri, D. Jiao, and K. Rajana, 'Lamb wave mode selection for increased sensitivity to interfacial weaknesses of adhesive bonds', In: Annual review of progress in quantitative NDE, Thompson DO, Chimenti DE eds., New York, Plenum Press, **12**:1579–1585, 1993.
31. R. E. Challis, U. Bork, and P. C. D. Todd, 'Ultrasonic NDE of adhered T-joints using Lamb waves and intelligent signal processing', *Ultrasonics*, **34**:445–459, 1996.
32. K. J. Sun, and P. H. Johnston, 'Mode conversions of Lamb waves for inspection of disbonds', *IEEE Ultrasonics Symposium*, 1992, pp. 763–766.
33. K. J. Sun, and P. H. Johnston, 'Feasibility of using Lamb waves for corrosion detection in layered aluminium aircraft structures', *IEEE Ultrasonics Symposium*, 1993, pp. 733–736.
34. K. J. Sun, and P. H. Johnston, 'Disbond detection in bonded aluminum joints using Lamb wave amplitude and time-of-flight', In: Annual review of progress in quantitative NDE, Thompson DO, Chimenti DE eds., New York, Plenum Press, **12**:1507, 1993.
35. K. J. Sun, and P. H. Johnston, 'Effect of rivet rows on propagation of Lamb waves in mechanically fastened two-layer aluminum plates', In: Annual review of progress in quantitative NDE, Thompson DO, Chimenti DE eds., New York, Plenum Press, **14**:1569–1575, 1995.
36. J. L. Rose, J. J. Ditri, D. Gallela, and T. Grant, 'Adhesive bond inspection utilizing ultrasonic Lamb waves', *15th Annual meeting of the adhesion society*, 1992, Hilton Head SC, pp. 181–183.
37. M. J. S. Lowe, C. W. Chan, and R. E. Challis, 'The transmission of Lamb waves across adhesively bonded lap joints', *Journal of the Acoustical Society of America*, **107**(3):1333–1345, 2000.
38. B. A. Auld, '*Acoustic Fields and Waves in Solids*', 1, Krieger Publishing Company, Florida, 1990.
39. R. B. Randall,'*Frequency Analysis*', Bruel and Kjaer, Naerum, Denmark, 1987.
40. R. J. Blake, 'Numerical models of Rayleigh wave scattering from surface features', PhD thesis, Dept of Electronic and Electrical Eng, University of London (University College), 1988.
41. R. P. Dalton, 'Propagation of acoustic emission signals in metallic fuselage structure', *JEE Proceedings—Science, Measurement and Technology*, 2001 (in press).
42. M. K. Hinders, 'Lamb wave scattering from rivets', In: Annual review of progress in quantitative NDE, Thompson DO, Chimenti DE eds., New York, Plenum Press, **15**:209–216, 1996.